International Journal of Automation and Computing 12(4), August 2015, 393-401
DOI: 10.1007/s11633-014-0858-6

Appropriate Sub-band Selection in Wavelet Packet Decomposition for Automated Glaucoma Diagnoses

Chandrasekaran Raja[1] Narayanan Gangatharan[2]

[1]Department of Electronics and Communication Engineering, Anjalai Ammal Mahalingam Engineering College, Kovilvenni, India

[2]Department of Electronics and Communication Engineering, R.M.K. College of Engineering and Technology, Puduvoyal 601206, India

Abstract: The most common reason for blindness among human beings is Glaucoma. The increase of fluid pressure damages the optic nerve which gradually leads to irreversible loss of vision. A technique for automated screening of Glaucoma from the fundal retinal images is presented in this paper. This paper intends to explore the significance of both the approximate and detail coefficients through wavelet packet decomposition (WPD). Decomposition is done with "db3" wavelet function and the images are decomposed up to level-3 producing 84 sub-bands. Two features, the energy and the entropy are calculated for each sub-band producing two feature matrices (158 images × 84 features). The above step is purely a statistical measure based on WPD. To enhance the diagnostic accuracy, the second phase considers the structural (biological) region of interest (ROI) in the image and then extracts the same features. It is worthy to note that direct biological features are not extracted to eliminate the drawbacks of segmentation whereas the biologically significant region is taken as biological-ROI. Interestingly, the detailed coefficient sub-bands (prominent edges) show more significance in the biological-ROI phase. Apart from enhancing the diagnostic accuracy by feature reduction, the paper intends to mark the significance indices, uniqueness and discrimination capability of the significant features (sub-bands) in both the phases. Then, the crisp inputs are fed to the classifier ANN. Finally, from the significant features of the biological-ROI feature matrices, the accuracy is raised to 85% which is notable than the accuracy of 79% achieved without considering the ROI.

Keywords: Glaucoma, wavelet packet decomposition, feature reduction, feature significance, artificial neural networks.

1 Introduction

Glaucoma is the fourth leading cause of blindness in India and is more prevalent in the aged people. Unlike cataract, the other major cause of blindness, the loss of vision caused by glaucoma cannot be regained. Besides old age, the other major cause for Glaucoma is family history, ethnic background, high intra-ocular pressure and high blood pressure[1].

Mookiah et al.[2] discussed the impact of glaucoma in human eyes: 1) Structural changes of the optic nerve head (ONH) and the nerve fibre layer and 2) simultaneous functional failure of the visual field. They have discussed the manifestation of structural changes by a slowly diminishing neuroretinal rim indicating the degeneration of the optic nerve.

The cost of glaucoma diagnoses through optical coherence tomography (OCT) and heidelberg retinal tomography (HRT) is not affordable for the large affected population[3]. Conventional digital fundus imaging is a relatively less expensive technique.

State-of-the-art glaucoma detection requires mass screening. Mookiah and Faust[4] discussed the necessity to automate glaucoma detection. The cost is reduced by mass screening. They have proposed that a small cost reduction per measurement will make a large difference. Furthermore, they compared the other modalities like HRT imaging which is very expensive because of skilled manpower and equipment cost.

Acharya et al.[5] extracted a variety of features linked to higher order spectra (HOS), co-occurrence matrix and difference-vector from the fundus images. Their exhaustive combination of features is classified by support vector machines, sequential minimal optimization and random forest. The texture and higher order spectral features have evolved as a remarkable feature set.

Discrete wavelet transform (DWT) is widely used to extract the texture features. DWT refers to the multi-band decomposition of the given image and can retrieve up to 98% energy of the original signal[6]. In DWT, only the previous approximation coefficients are decomposed. However, using wavelet packet decomposition (WPD), both the approximate and detailed coefficients are decomposed. Hence, WPD is widely used in image processing and pattern recognition[7].

As mentioned in [8], the dominant texture features are available in the detailed coefficient sub-bands, the WPD is a better technique to extract the texture features than the conventional DWT. They revealed that the dominant texture features are available in the horizontal bands which belong to the detailed sub-bands. It implies that the detailed coefficient sub-band is useful in discriminating types of tumour from ultrasound images. In fact, the work in [8] does not decompose the approximate coefficient sub-bands

Regular paper
Manuscript received October 28, 2013; accepted April 2, 2014
Recommended by Associate Editor Giuliano Premier

at all.

More than the decomposition style, DWT or WPD, the choice of suitable wavelet filter is important. The prominence of the Daubechies wavelets for the WPD based feature extraction is evident from the work done in [9]. Huang and Aviyete[9] iterated the prominence of the "db" wavelet base in their mutual information based sub-band selection (MISS) for WPD based feature extraction.

The work done by Dua et al.[10] establishes the discriminatory potential of the Daubechies (db3) wavelet base in glaucoma diagnoses. Based on the p-value, "db3" wavelet is chosen from a set of wavelet bases. Further, the difference between two adjacent orders of the same wavelet function is insignificant as they are analogous to each other[11].

Koh et al.[12] developed an automated glaucoma detection system using discrete wavelet transform (DWT) based features. The work relies on the information content in the relative energy and entropy based features. They have discussed the superiority of statistical methods of feature extraction over the segmentation methods.

Regarding WPD, since more number of features are extracted, feature selection is a crucial issue. In general, in feature selection methods like principle component analysis and linear discriminant analysis, it is required to decompose all the sub-bands in both the training and testing phases, whereas in the feature selection among the wavelet components, the image can be decomposed only for the significant sub-bands[9].

In [13], entropy feature is extracted and the discrimination capability of the features is measured. The features that possess the discrimination capability are only decomposed further. In this way, any significant sub-band with insignificant parent will not be given due-significance. The work in [9] broadly classifies the feature selection among the wavelet features into two methods. Firstly, the dependency is measured among the sub-bands only if the sub-bands belong to the same family[14]. Secondly, all the features are extracted and the significance is measured globally[15].

If the statistical dependence between the sub-bands is not considered, the classification performance is degraded. In [16], the sub-band selection is based on the entropy cost function, where the entropy variation caused by the children nodes is compared with that of the parent node. In [17], only one sub-band is selected from each subset (family) based on the dependency measured whereas the proposed methodology clearly shows that the sub-bands from the same family are significant.

An image is decomposed only for the sub-bands selected by the feature selection[17]. After feature selection is done, in wavelet packet decomposition, it is not required to decompose all the sub-bands.

In this work, the 2D discrete wavelet packet transform is implemented using the "db3" wavelet base for the fundus images up to level 3 producing 84 sub-bands.

We have used Daubechies wavelets to extract the statistical features from the images. The wavelets form an orthonormal basis. The energy spectrum is concentrated around the low frequencies[18], which make them appropriate for texture based classification task.

Energy and entropy are the two features measured for all the sub-bands for both the phases.

The methodology incorporated in this work to measure the significance globally is convincing, as the statistical dependence occurs in all the families. In other word, the variation of entropy caused by the inclusion of a particular feature "f" is degraded by its own family and the capability of each feature to increase the entropy overcoming its own family is measured as uniqueness.

2 Proposed glaucoma detection in fundal retinal images

The block diagram of the proposed technique is given in Fig. 1. It shows the different phases involved and the operations in each phase.

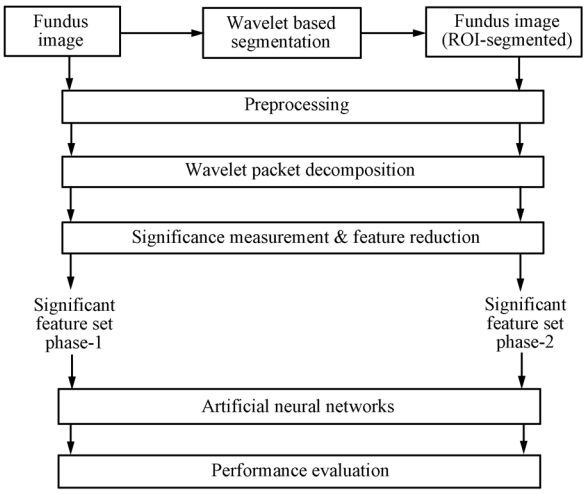

Fig. 1 Block diagram of the proposed technique

2.1 Inputs

The fundus images are collected from the rim-one database for both the normal and glaucoma images. The statistical phase considers the statistical features for the entire spatial span of the image. To enhance the diagnostic accuracy, in the second phase, the optical disc region (biological ROI) is segmented in the images and the statistical features are extracted from the biological region of interest alone.

2.1.1 Wavelet based segmentation

In [2], segmentation is done by grey level threshold of red and green components of the fundus images to segment the disc and cup respectively. In this work, the idea to threshold in the wavelet domain is extended instead of the grey levels in spatial domain. The steps are sequentially as follows. The first level approximate wavelet coefficients of the images are extracted. As most of the energy is preserved in the approximate coefficient sub-bands, we choose the same sub-band (level-1) for carrying out the segmentation by thresh-

olding. Fig. 2 (a) shows an image corresponding to the first level approximate coefficients of the glaucoma image.

(a) Approximate wavelet-coefficient image (b) Disc segmented approximate wavelet-coefficient image (c) Disc segmented image

Fig. 2 Wavelet based segmentation

The value of the wavelet approximate coefficients corresponding to the disc region and the surrounding regions are inspected manually for both the classes. Several thresholds are experimented and the optimal threshold suitable to both the classes is selected. Since the size of the disc is not extracted, as a direct biological feature, we have not spent the computational heads towards the accuracy in segmentation. Eventually, the optical disc is segmented with minimal neighboring pixels. On the other hand, the inclusion of optical disc completely in the ROI is ensured.

The final metrics show that the texture features of the optical disc (with minimal neighborhood) is more dominant in classifying than the same features of entire image.

Fig. 2 (b) shows the first level approximate coefficient image segmented for optical disc (with least neighborhood) by using the optimal threshold.

The segmented images of the first level approximate coefficients are subjected to inverse wavelet transform to reconstruct the segmented optical disc (with least-neighborhood) in the original image.

Fig. 2 (c) shows the images corresponding to segmented optical disc with neighborhood by using the optimal threshold.

2.2 Pre-processing phase

Initially, the fundus images corresponding to both the statistical and biological-ROI phases are pre-processed so as to make the images fit for further processing. Through pre-processing, the noise is reduced and image is enhanced. Grey scale conversion and histogram equalization are carried out in this phase.

2.2.1 Grey scale conversion

A grey-scale image is an image which is composed exclusively of shades of grey, varying from black at the weakest intensity to white at the strongest. This range is represented in an abstract way ranging from 0 (total absence, black) to 1 (total presence, white).

2.2.2 Histogram equalization

It improves the dynamic range of the histogram of the image and assigns the intensity values of the pixels in the input image such that the output image contains uniform distribution of intensities thus enhancing the feature extraction process.

2.3 Wavelet packet decomposition

The 2D-discrete WPD of an image $I(x, y)$ is accomplished with the "db3" wavelet base. The decomposition is done for 3 levels for both the phases, yielding 84 sub-bands. Energy and entropy are the two features measured for all the sub-bands in both the phases.

Four sub-images are obtained for every decomposition, the approximate and detailed (horizontal, vertical, diagonal) coefficients are given respectively from (1) to (4).

$$I^l_{k(i,j)} = \sum_x \sum_y h(x)h(x)I^{l-1}_{\frac{k}{4},(x+2i,y+2j)} \tag{1}$$

$$I^l_{k+1(i,j)} = \sum_x \sum_y h(x)g(x)I^{l-1}_{\frac{k}{4},(x+2i,y+2j)} \tag{2}$$

$$I^l_{k+2(i,j)} = \sum_x \sum_y g(x)h(x)I^{l-1}_{\frac{k}{4},(x+2i,y+2j)} \tag{3}$$

$$I^l_{k+3(i,j)} = \sum_x \sum_y g(x)g(x)I^{l-1}_{\frac{k}{4},(x+2i,y+2j)}. \tag{4}$$

The transfer functions $h(\cdot)$ and $g(\cdot)$ represent the low-pass and high-pass filter kernels. In (1)–(4), i and j are the translational variables along the horizontal and vertical directions respectively.

The wavelet packet tree in Fig. 3 shows the level-1 decomposition. The $L(Z)$ and $H(Z)$ are the low pass and high pass filters correspondingly. The output of level-1 decomposition consists of 4 sub-bands (A, H, V and D) which are the approximate, horizontal, vertical and diagonal coefficients respectively. Unlike DWT, here all the 4 sub-bands of level-1 are decomposed producing 16 sub-bands at level-2 and 64 sub-bands at level-3. Thus, 84 sub-bands are extracted for both the statistical and biological-ROI phase of all the images.

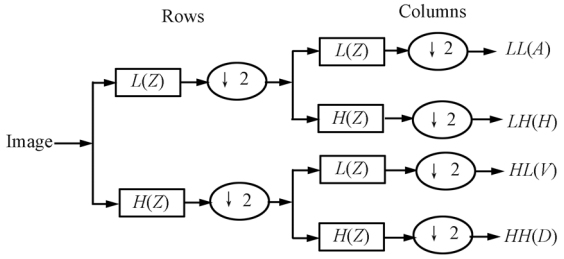

Fig. 3 Wavelet packet decomposition tree (shown for 1 level)

The evidence for the ability of the WPD to discriminate texture better than discrete wavelet transform is [8]. Tsiaparas et al.[8] concluded that the dominant texture features exhibit horizontal directionality.

In addition to establishing the discriminatory significance of the detailed coefficient (wavelet) sub-bands, this work makes a deeper venture to mark the significance indices of individual sub-bands. Then, a crisp set of significant sub-bands is used for classification.

2.3.1 Energy feature

The energy of each sub-band $I(x, y)$ provides a measure of the response of the image to the specific scale and orien-

tation of the filters[17].

The energy is calculated for each sub-band as

$$E(\beta) = \frac{1}{p^2 + q^2} \sum_{x=p} \sum_{y=q} |I(x, y)|^2 \quad (5)$$

where β is one of the 84 sub-bands with p-rows and q-columns. Energy is calculated also for phase-2, discarding the pixels outside the biological-ROI.

2.3.2 Entropy feature

The measurement of the randomness of the grey levels of a sub-band $I(x, y)$ provides a qualitative measure of the texture.

$$Entropy(\beta) = -\sum_{i=1}^{p \times q} p_i \log_2 p_i. \quad (6)$$

In (6), the entropy is measured for all the pixels, $i = 1$ to $(p \times q)$, and p_i is the probability of occurrence of the i-th pixel.

Entropy is calculated also for phase-2, discarding the pixels outside the biological-ROI.

3 Feature extraction, significance measurement and feature reduction

3.1 Feature extraction

Four feature matrices are available namely, the energy feature matrices and the entropy feature matrices for both the statistical and biological-ROI phases of operation. The corresponding MAT-files are

1) Energy feature matrix of statistical phase;
2) Entropy feature matrix of the statistical phase;
3) Energy feature matrix of biological-ROI phase;
4) Entropy feature matrix of biological-ROI phase.

All the four matrices are 158×85 of size.

3.2 Significance measurement

The feature reduction is based on 2 significant measures, the uniqueness of a feature with respect to the other features and the discrimination capability of the feature to categorize between the classes.

Krishnan and Faust[4] removed the features that are not random enough among the set, i.e., the features that do not increase the entropy above a threshold by their inclusion in the set. In this work, we term those features that significantly increase the entropy, by their inclusion, as "unique".

Huang and Aviyente[9] assessed whether the two classes have different mean for each feature. In this work, the features with significant mean-difference between the classes are termed as "discriminatory significant".

A set of n features is given as

$$F = \bigcup_{j=1}^{n} f_j. \quad (7)$$

Uniqueness of a particular feature f is measured by calculating the variation of entropy caused by the inclusion of that particular feature to the feature set. First, the whole entropy ENT is measured calculating the entropy of all the features as a feature vector,

$$ENT = entropy\left(\bigcup_{j=1}^{n} f_j\right). \quad (8)$$

As there are m images ($i = 1, \cdots, m$) and $m = 158$, the whole entropy is calculated for all the images. Thus, a whole entropy vector is created as

$$ENT_i = \{ENT_1, ENT_2, \cdots, ENT_m\}. \quad (9)$$

Then, the uniqueness of a particular feature f_p, $1 \le p \le n$ is calculated by eliminating that particular feature f_p for all the images and then calculating the entropy. Considering f'_p as the feature set excluding the p-th feature f_p,

$$Entropy(f'_p) = Entropy\left[\bigcup_{j=1}^{p-1} f_j \quad \text{and} \quad \bigcup_{j=p+1}^{n} f_j\right]. \quad (10)$$

$Entropy(f'_p)_i$ is the entropy vector, then is evaluated for all the i images without the feature f_p. The uniqueness of any feature f_p is defined as

$$Uniqueness(f_p) = ENT_i - Entropy(f'_p)_i. \quad (11)$$

Discrimination capability is the measure of a particular feature to categorize between the classes.

Let F_i be any of the feature matrices. It is the row-wise appending of the feature-vectors F specified in (7). To evaluate the discrimination capability of the features, each feature matrix is broken into two. This is accomplished by indexing the clinically determined normal and glaucomatous images with different values.

Based on the index, the feature matrices F_i are termed as F_{norm} and F_{glauc} that correspond to normal and glaucomatous images. The discriminatory significance of j-th feature (between the classes) is measured in (12) as $Discr(F_j)$.

$$Discr(F_j) = mean(F_{\text{norm}})_j - mean(F_{\text{glauc}})_j. \quad (12)$$

3.3 Feature reduction

In the feature reduction process for all the 4 matrices, the features are arranged in the order of decreasing significance discarding the insignificant features. The discard is done such that individual features with the significance index above the mean of the significance indices of all the features are considered. The percentage of the significance is calculated by assigning the maximum value of 100% to the feature with maximum significance.

Table 1 shows the features with the energy of the intensities of the sub-bands which are arranged in the order of decreasing significance with maximum significant feature (AAA) to the least significant feature (HAD), as the insignificant features below the same are discarded. Columns 4 and 5 give the percentage of significance (uniqueness and discrimination, respectively). The last column shows the usefulness of a sub-band as a parent.

Table 2 shows the feature reduction done to the entropy features. The average of the 2 significance indices (uniqueness and discrimination capability) is not calculated as the significance lies in the complementary sub-bands.

Table 1 Feature reduction for energy feature matrix of statistical phase
(U is uniqueness of the energy feature, D is discriminatory significance of energy feature)

Wavelet sub-band	U	D	U (%)	D (%)	Average (U (%) & D (%))	Significance-further decomposition
AAA	0.022	21.50	100	100	100	Level 4 not estimated
AA	0.022	9.45	100	43.95	71.97	100%
A	0.022	4.51	100	20.99	60.49	75%
HD	0.019	0.004	88.5	0.019	44.28	50%
AVV	0.016	0.025	73.2	0.11	36.66	Level 4 not estimated
AAV	0.015	0.049	66.7	0.22	33.50	Level 4 not estimated
AVA	0.014	0.002	63.9	0.009	31.97	Level 4 not estimated
HAH	0.0124	0.001	56	0.005	28.03	Level 4 not estimated
AAH	0.012	0.005	53.51	0.025	26.76	Level 4 not estimated
AHD	0.011	0.008	49.570	0.038	24.80	Level 4 not estimated
AHH	0.010	0.032	44.830	0.152	22.49	Level 4 not estimated
AHA	0.009	0.008	43.368	0.040	21.70	Level 4 not estimated
HHA	0.009	0.014	42.304	0.068	21.18	Level 4 not estimated
VVV	0.009	0.0001	41.915	0.0004	20.95	Level 4 not estimated
VAV	0.009	0.0018	41.267	0.008	20.63	Level 4 not estimated
ADD	0.008	0.0062	38.546	0.028	19.29	Level 4 not estimated
HHH	0.007	0.0084	34.870	0.039	17.45	Level 4 not estimated
VVA	0.007	0.0005	34.341	0.002	17.17	Level 4 not estimated
ADV	0.007	0.0045	33.743	0.020	16.88	Level 4 not estimated
AV	0.007	0.0028	33.483	0.013	16.74	100%
HDV	0.007	0.0033	32.911	0.015	16.46	Level 4 not estimated
VVH	0.007	0.0075	32.735	0.034	16.38	Level 4 not estimated
AVD	0.007	0.0085	31.224	0.039	15.63	Level 4 not estimated

Table 2 Feature reduction for entropy feature matrix of statistical phase
(U is uniqueness of the entropy feature, D is discriminatory significance of entropy feature)

Wavelet sub-band	U	D	U (%)	D (%)	Significance-further decomposition
ADH	–	0.31	–	100	Level 4 not estimated
AD	–	0.31	–	100	100 %
VVH	–	0.29	–	94.43	Level 4 not estimated
VDH	–	0.29	–	92.98	Level 4 not estimated
ADA	–	0.29	–	92.19	Level 4 not estimated
ADV	–	0.28	–	89.66	Level 4 not estimated
AVH	–	0.28	–	89.00	Level 4 not estimated
HDV	–	0.27	–	85.62	Level 4 not estimated
VD	–	0.26	–	82.49	100%
VV	–	0.25	–	81.16	50%
HAD	–	0.25	–	80.22	Level 4 not estimated
VDD	–	0.25	–	79.87	Level 4 not estimated
VDA	–	0.2463	–	77.81	Level 4 not estimated
ADD	–	0.2401	–	75.86	Level 4 not estimated
VVD	–	0.23	–	75.32	Level 4 not estimated
AA	0.058	–	100	–	Level 4 not estimated
A	0.058	–	100	–	Level 4 not estimated

Table 3 Feature reduction for energy feature matrix of biological-ROI phase

Wavelet sub-band	U	D	U (%)	D (%)	Significance (%)
AAA	0.083	0.13	93.47	100	96.73
AA	0.0825	0.06	92.80	46.17	69.48
A	0.088	0.02	100	22.28	61.14

Table 3 shows similar feature reduction done to the energy feature of the biological-ROI phase. Only 3 sub-bands are significant. Tables 4 and 5 show the similar feature reduction done to the entropy feature of the biological-ROI

phase. Thirty-nine sub-bands (forty-six percentage of the sub-bands obtained by 3-level decomposition) are significant. Like the entropy features of phase-1, the average of the 2 significance indices (uniqueness and discrimination capability) is not calculated as the significance lies in the complementary sub-bands.

Table 4 Feature reduction for entropy feature matrix of biological-ROI phase-uniqueness

Wavelet sub-band	U	U (%)
DAA	0.0329	100
DAD	0.0318	96.65
DA	0.0304	92.40
DD	0.0304	92.40
DHH	0.0304	92.40
DAH	0.0302	91.79
DAV	0.0299	90.88
DHA	0.0298	90.57
DH	0.0291	88.44
DVV	0.0291	88.44
DV	0.029	88.14
DVD	0.029	88.14
VHA	0.0289	87.84
DVA	0.0289	87.84
HVA	0.0285	86.62
HVV	0.0285	86.62
D	0.0279	84.80
DHD	0.0275	83.58
DVH	0.0271	82.37
H	0.0269	81.76
VH	0.0267	81.15
V	0.0265	80.54
HV	0.0262	79.63
VHH	0.0259	78.72
DHV	0.0257	78.11
DDD	0.0252	76.59
HAV	0.0227	68.99
VAH	0.0211	64.13
DDV	0.0207	62.91
VA	0.019	57.75
HA	0.0186	56.53
DDH	0.0173	52.58

Table 5 Feature reduction for entropy feature matrix of biological-ROI phase-discriminatory significance

Wavelet sub-band	D	D (%)
AAA	0.202	100
AA	0.200	98.96
AAV	0.176	87.19
AVA	0.167	82.69
AAD	0.161	79.82
AAH	0.159	78.83
AVV	0.158	78.48

Thus, the four feature matrices (energy, entropy feature matrices of the statistical and biological-ROI phases, as listed in Section 3.1) are feature reduced using (11) and (12). The number of features selected out of these feature matrices are 23, 17, 3, 39, respectively. The four feature reduced matrices are concatenated column-wise to get a significant feature matrix (158 × 82). Then, each feature vector in the matrix is normalized before classification.

4 Classification by ANN

Artificial neural networks (ANN) are used for the classification task. In this work, 85 input layers and 20 hidden layers are used in the gradient descent algorithm. In [19], conjugate gradient descent algorithm is employed and classification of normal and glaucomatous images is done. Gradient descent is a first-order optimization algorithm. To find the local minimum of a function using gradient descent, steps are taken proportional to the negative of the gradient of the function at the current point. In order to train the neural networks, the gradient G of the loss function is computed with respect to each weight W_{ji} of the network. It shows the fact that small change in that weight will affect the overall error E_r. Initially, loss function is divided into separate terms for each point s in the training data.

$$E_r = \sum_s E_r^s \tag{13}$$

$$E_r^s = \frac{1}{2}\sum_k (t_k^s - y_k^s) \tag{14}$$

where k ranges over the output units of the network for the actual output y and the target t. The gradient is split into separate components for each training point as

$$G = \frac{\partial E_r}{\partial w_{ij}} = \sum_s \frac{\partial E_r^s}{\partial w_{ij}}. \tag{15}$$

Using the chain rule to decompose the gradient into two factors, we get

$$\frac{\partial E_r}{\partial w_{ki}} = \frac{\partial E}{\partial y_k}\frac{\partial y_k}{\partial w_{ki}} = -(t_w - y_w)y_i. \tag{16}$$

The subscripts j, i and k index the input, hidden and the output layers, respectively, and t_w and y_w refer to the target and the actual outputs respectively at the hidden layer. To find the gradient G for the entire data set, summation at each weight is taken for all the data points. Subsequently, small proportion μ (called the learning rate) is subtracted out of G from the weights to perform gradient descent. Steepest gradient algorithm is carried out by initialising all weights to small random values. Then for all weights w_{ij}, Δw_{ij} is set as zero. Then for each data point, the weights are modified according to the equation $\Delta w_{ij} = \Delta w_{ij} + (t_i - y_i)y_j$. Once this is carried out for all the data points, the weight is set as $w_{ij} = w_{ij} + \mu\Delta w_{ij}$.

The algorithm terminates once it is sufficiently near the minimum of the error function where $G = 0$, and then it can be concluded that the algorithm has converged.

5 Results and discussions

5.1 Analysis about the energy feature matrix of the statistical phase

Column 1 of Table 1 shows the wavelet features. Out of the 84 features, only 23 features (27%) are selected as significant. Only the approximate coefficients of all the 3 levels (A, AA, AAA) exhibit the discriminatory significance. Though the remaining 20 significant features exhibit least discrimination capability, their combined uniqueness will be able to discriminate. The features that exhibit discrimination form the subset of the features that exhibit uniqueness. The last column of Table 1 shows the significance of each sub-band as a parent, i.e., the value of 100% significance of AA means that all its children (AAA, AAH, AAV, AAD) are significant.

5.2 Analysis about the entropy feature matrix of the statistical phase

Column 1 of Table 2 shows the wavelet features that are significant. Out of the 84 features, only 17 features (20%) are selected as significant. The approximate coefficients of levels 1 and 2 have the same maximum uniqueness (A, AA) whereas the level 3 approximate coefficient (AAA) is not unique.

Entropy feature matrix has produced 15 sub-bands with enough discrimination. Measuring the discrimination capability, the entropy feature matrix has produced significant sub-bands from both the approximate and detailed coefficients.

The sub-bands that exhibit uniqueness and discrimination are complementary.

5.3 Analysis about the energy feature matrix of the biological-ROI phase

After incorporating the region of interest in the images, as shown in Table 3, the number of sub-bands, with significant energy features, drastically reduced to three. This provides a subjective insight that the energy of intensities of the segmented optical disc does not vary significantly between different wavelet sub-bands of the same image and also between a normal image and diseased image.

5.4 Analysis about the entropy feature matrix of the biological-ROI phase

Contrary to the property of the energy features of the segmented optical disc, as shown in Tables 4 and 5, the entropy features produce 32 unique sub-bands and 7 sub-bands are of discriminatory significance. Totally, 49% of the entropy features of the biological-ROI phase are significant giving an insight that the entropy is significant in the biological-ROI phase. The entropy difference as in (11) varies significantly between the detailed coefficient sub-bands of the same image. In other word, the entropy features of the detailed co-efficient sub-bands are unique. The entropy also varies between the approximate co-efficient sub-bands of the normal and diseased images, i.e., the entropy features of the approximate co-efficient sub-bands are discriminatory.

Table 6 provides a summary of inferences quoted in Section 5. Inferring Table 6 for the biological-ROI phase, only 3 and 39 sub-bands are significant from the energy and the entropy features respectively. Thus, a crisp feature set (feature to image ratio is 26%) is fed to the classifier.

The importance of considering both the structural and statistical content of an image in the phase-2 of our work can be emphasized by comparing with other works that solely rely on either structural or statistical content of an image. The work done in [20] solely relies on the cup-to-disc ratio (structural content) and produced a specificity of 87%. The work done in [3] solely relies on the statistical content of an image which produced an accuracy of 82.5%. Since both statistical and structural content of the images are considered, the proposed algorithm has overcome the above said results with the specificity of 100% and the accuracy of 85%.

The importance of the detailed co-efficient sub-bands is evident from the comparison with our previous work [16]. An accuracy of 81% is produced without decomposing the detailed coefficient sub-bands. In this work, a 4% raise in accuracy is achieved (in comparison with [16]), by decomposing the detailed coefficient sub-bands also.

Table 7 provides a summary of the results achieved in glaucoma diagnoses by other researchers using conventional discrete wavelet transform, complex wavelet transform and wavelet packets. Several other segmentation based methods are also compared.

6 Performance evaluation

The bar chart in Fig. 4 shows the results of the algorithm for the statistical (STAT) and B-ROI phases with the three metrics, i.e., accuracy, sensitivity and specificity. In order to find these metrics, we first compute some of the terms like, true positive (TP), true negative (TN), false negative (FN) and false positive (FP).

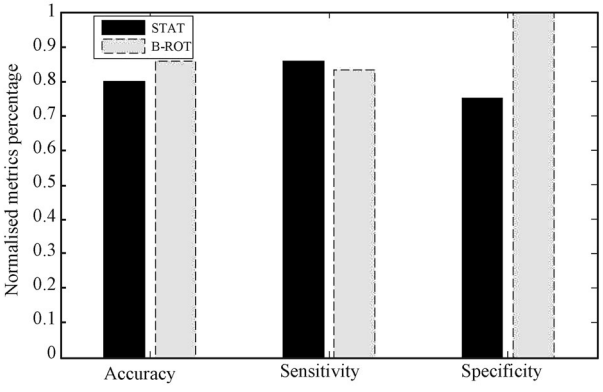

Fig. 4 Performance evaluation graph for the statistical and biological-ROI phase

Table 6 Summary of conclusions

	Phase-1 (statistical phase) Feature reduction–40/168 features (24%)				Phase-2 (biological-ROI phase) Feature reduction–41/168 features (24%)			
	Energy (23/84) 27%		Entropy (17/84) 20%		Energy (3/84) 3%		Entropy (39/84) 46%	
	U	D	U	D	U	D	U	D
Number of significant features	23	3	2	15	3	3	32	7
Comparison between U & D significant sub-bands	D is a subset of U		U & D are complementary		U & D have the same 3 features		U & D are complementary	
Number of approximate & detailed coefficients	A-14 D-9	A-3 D-0	A-2 D-0	A-6 D-9	A-3 D-0	A-3 D-0	A-0 D-32	A-7 D-0

Table 7 Comparison of other glaucoma detection techniques

Reference	Features	Classifier	Performance measure	Performance measure of the proposed method
[19]	Higher order spectra and complex wavelet transform	ANN (conjugate gradient descent)	Accuracy: 81% Sensitivity: 87% Specificity: 87%	Accuracy: 85% Sensitivity: 82% Specificity: 100%
[20]	Cup-to-disc ratio	CDR threshold	Sensitivity: 87% Specificity: 82%	
[3]	Cup-to-disc ratio, blood vessel orientation	ANN	Sensitivity: 100% Specificity: 80%	
[8]	Discrete wavelet transform, wavelet packets and gabor transform	SVM and probabilistic neural networks	Average accuracy: 82.5%	
[2]	Higher order spectra and discrete wavelet transform	SVM (support vector machines)	Accuracy: 95% Sensitivity: 93.3% Specificity: 96.67%	

Zhu et al.[21] described the metrics as follows. Sensitivity is the proportion of true positives that are correctly identified by a diagnostic test. It shows how good the test is at detecting a disease. Specificity is the proportion of the true negatives correctly identified by a diagnostic test. It suggests how good the test is at identifying normal (negative) condition. Accuracy is the proportion of true results, either true positive or true negative, in a population. It measures the degree of truthfulness of a diagnostic test on a condition. These can be expressed in the terms of TP, FP, FN and TN by

$$\text{Sensitivity} = \frac{\text{TP}}{\text{TP} + \text{FN}}$$
$$\text{Specificity} = \frac{\text{TN}}{\text{TN} + \text{FP}}$$
$$\text{Accuracy} = \frac{\text{TN} + \text{TP}}{\text{TN} + \text{TP} + \text{FN} + \text{FP}}.$$

From the bar chart in Fig. 4, it is evident that the algorithm yields 78% accuracy, 85% sensitivity and 75% specificity in the statistical phase. Considering the biological-ROI alone in the next phase, the performance is raised to 85% accuracy, 82% sensitivity and 100% specificity.

7 Conclusions

This work emphasizes on the significance of the detailed coefficient sub-bands in the feature extraction process. This work also proposes a novel method of selecting the biological-ROI and then evaluating the statistics. The accuracy can be further improved by designing optimal wavelet filter coefficients.

References

[1] Y. Mallikarjun. Two molecular mechanisms causing glaucoma found, [Online], Available: http://www.thehindu.com/sci-tech/health/two-molecular-mechanisms-causing-glaucoma-found / article4902049 . ece, July 10, 2013.

[2] M. R. K. Mookiah, U. R. Acharya, C. M. Lim, A. Petznick, J. S. Suri. Data mining technique for automated diagnosis of glaucoma using higher order spectra and wavelet energy features. *Knowledge-based Systems*, vol. 33, no. 1, pp. 73–82, 2012.

[3] J. Nayak, U. R. Acharya, P. S. Bhat, N. Shetty, T. C. Lim. Automated diagnosis of glaucoma using digital fundus images. *Journal of Medical Systems*, vol. 33, no. 5, pp. 337–346, 2009.

[4] M. R. K. Mookiah, O. Faust. Automated glaucoma detection using hybrid feature extraction in retinal fundus im-

ages. *Journal of Mechanics in Medicine and Biology*, vol. 13, no. 1, Article number 1350011, 2013.

[5] U. R. Acharya, S. Dua, X. Du, S. V. Sree, C. K. Chua. Automated diagnosis of glaucoma using texture and higher order spectra features. *IEEE Transactions on Information Technology in Biomedicine*, vol. 15, no. 3, pp. 449–455, 2011.

[6] R. S. Asamwar, K. M. Bhurchandi, A. S. Gandhi. Interpolation of images using discrete wavelet transform to simulate image resizing as in human vision. *International Journal of Automation and Computing*, vol. 7, no. 1, pp. 9–16, 2010.

[7] X. Yang. Wear state recognition of drills based on K-means cluster and radial basis function neural network. *International Journal of Automation and Computing*, vol. 7, no. 3, pp. 271–276, 2010.

[8] N. N. Tsiaparas, S. Golemati, I. Andreadis, J. S. Stoitsis, I. Valavanis, K. S. Nikita. Comparison of multiresolution features for texture classification of carotid atherosclerosis from B-mode ultrasound. *IEEE Transactions on Information Technology in Biomedicine*, vol. 15, no. 1, pp. 130–137, 2011.

[9] K. Huang, S. Aviyente. Wavelet feature selection for image classification. *IEEE Transactions on Image Processing*, vol. 17, no. 9, pp. 1709–1770, 2008.

[10] S. Dua, U. R. Acharya, P. Chowriappa, S. VinithaSree. Wavelet-based energy features for glaucomatous image classification. *IEEE Transactions on Information Technology in Biomedicine*, vol. 16, no. 1, pp. 80–87, 2012.

[11] A. M. Hasan, K. Samsudin, A. R. Ramli. Intelligently tuned wavelet parameters for GPS/INS error estimation. *International Journal of Automation and Computing*, vol. 8, no. 4, pp. 411–420, 2011.

[12] J. E. W. Koh, M. R. K. Mookiah, N. A. Kadri. Application of Multiresolution analysis for the detection of glaucoma. *Journal of Medical Imaging and Health Informatics*, vol. 3, no. 3, pp. 401–408, 2013.

[13] N. Rajpoot. Local discriminant wavelet packet basis for texture classification. In *Proceedings of SPIE, Wavelets: Applications in Signal and Image Processing* X, Bellingham, USA, vol. 5207, pp. 774–783, 2003.

[14] G. L. Fan, X. G. Xia. Wavelet-based texture analysis and synthesis using hidden Markov models. *IEEE Transactions on Circuits and Systems–I: Fundamental Theory and Applications*, vol. 50, no. 1, pp. 106–120, 2003.

[15] H. Chen, P. Varshney. Feature subset selection with applications to hyperspectral data. In *Proceedings of IEEE International Conference on Acoustics, Speech, Signal Processing*, IEEE, Syracuse, USA, vol. 2, pp. 249–252, 2005.

[16] R. R. Coifman, M. V. Wickerhauser. Entropy-based algorithms for best basis selection. *IEEE Transactions on Information Theory*, vol. 38, no. 2, pp. 713–718, 1992.

[17] K. Huang, S. Aviyente. Statistical partitioning of wavelet subbands for texture classification. In *Proceedings of International Conference on Image Processing*, IEEE, Michigan State University, East Lansing, USA, vol. 1, pp. I-441–I-444, 2005.

[18] S. Z. Mahmoodabadi, A. Ahmadian, M. D. Abolhasani. ECG feature extraction using daubechies wavelets. In *Proceedings of the 5th IASTED International Conference on Visualization, Imaging and Image Processing*, Spain, pp. 343–348, 2005.

[19] C. Raja, N. Gangatharan. Glaucoma detection in fundal retinal images using trispectrum and complex wavelet-based features. *European Journal of Scientific Research*, vol. 97 no. 1, pp. 159–171, 2013.

[20] C. Muramatsu, T. Nakagawa, A. Sawada, Y. Hatanaka, T. Yamamoto, H. Fujita, Automated determination of Cup-to-disc ratio for classification of glaucomatous and normal eyes on stereo retinal fundus images. *Journal of Biomedical Optics*, vol. 16, no. 9, Article number 096009, 2011.

[21] W. Zhu, N. Zeng, N. Wang. Sensitivity, specificity, accuracy, associated confidence interval and ROC analysis with practical SAS Implementations. In *Proceedings of the NESUG Health Care and Life Sciences, Baltimore, USA*, pp. 1–9, 2010.

Chandrasekaran Raja received the B. Eng. degree in electronics and communication engineering from Bharathidasan University, India in 2003, and the M. Tech. degree in biomedical signal processing and instrumentation from Shanmugha Arts, Science, Technology and Research Academy University, India. He is a Ph. D. candidate from Anna University, India. From 2005 to 2014, he has been working as an assistant professor in various engineering colleges in India. Since 2013, he has been working as an assistant professor, Department of Electronics and Communication Engineering, Anjalai Ammal Mahalingam Engineering College, India. To his credit, he has published three research paper in international journal and national level conference proceedings.

His research interests include digital signal processing and image processing.

E-mail: rajachandru82@yahoo.co.in (Corresponding author)
ORCID iD: 0000-0001-7351-3403

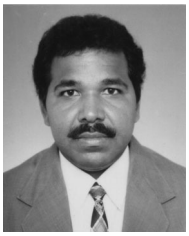

Narayanan Gangatharan received the B. Eng. degree in electronics and communication engineering in 1988, and the M. Eng. degree in microwave and optical engineering in 1990, both from Madurai Kamaraj University, India. He is the second ranker in the M. Eng. degree examinations of Madurai Kamaraj University, India in 1990. He received his second M. Eng. degree in computer science and engineering from Manonmaniam Sundaranar University, Tirunelveli, India in 1997, and his MBA degree in Finance and Marketing from Madurai Kamaraj University, India in 1999. From 1997 to 2001, he was a professor in the Faculty of Electronics and Communication Engineering at the Indian Engineering College, India. From 2001 to 2005, he was on the Faculty of Engineering, Multimedia University (MMU), Cyberjaya Campus Malaysia. From 2005 to 2006, he was on the Faculty of Electrical Engineering, Universiti Teknologi MARA (UiTM), Shah Alam in Malaysia. He took his Ph. D. degree in telecommunication engineering from Multimedia University in Malaysia. From January 2007 to January 2009, he was on the Faculty of Engineering at the Kigali Institute of Science and Technology (KIST), Kigali, Rwanda. From February 2009 to September 2010, he was an Information and Communication Technology Consultant at Rwanda Utilities Regulatory Agency (RURA), Rwanda. Since September 2010, he has been working as a professor & head in Department of Electronics and Communication Engineering, RMK College of Engineering & Technology, India. To his credit, he has published more than 25 research papers in international journals and conference proceedings.

His research interests include two dimensional and multidimensional digital signal processing, image processing, multimedia coding and telecommunication.

E-mail: n.gangatharan@yahoo.com
ORCID iD: 0000-0003-3948-5722